iScience

CellPress
OPEN ACCESS

Article

A human cornea-on-a-chip for the study of epithelial wound healing by extracellular vesicles

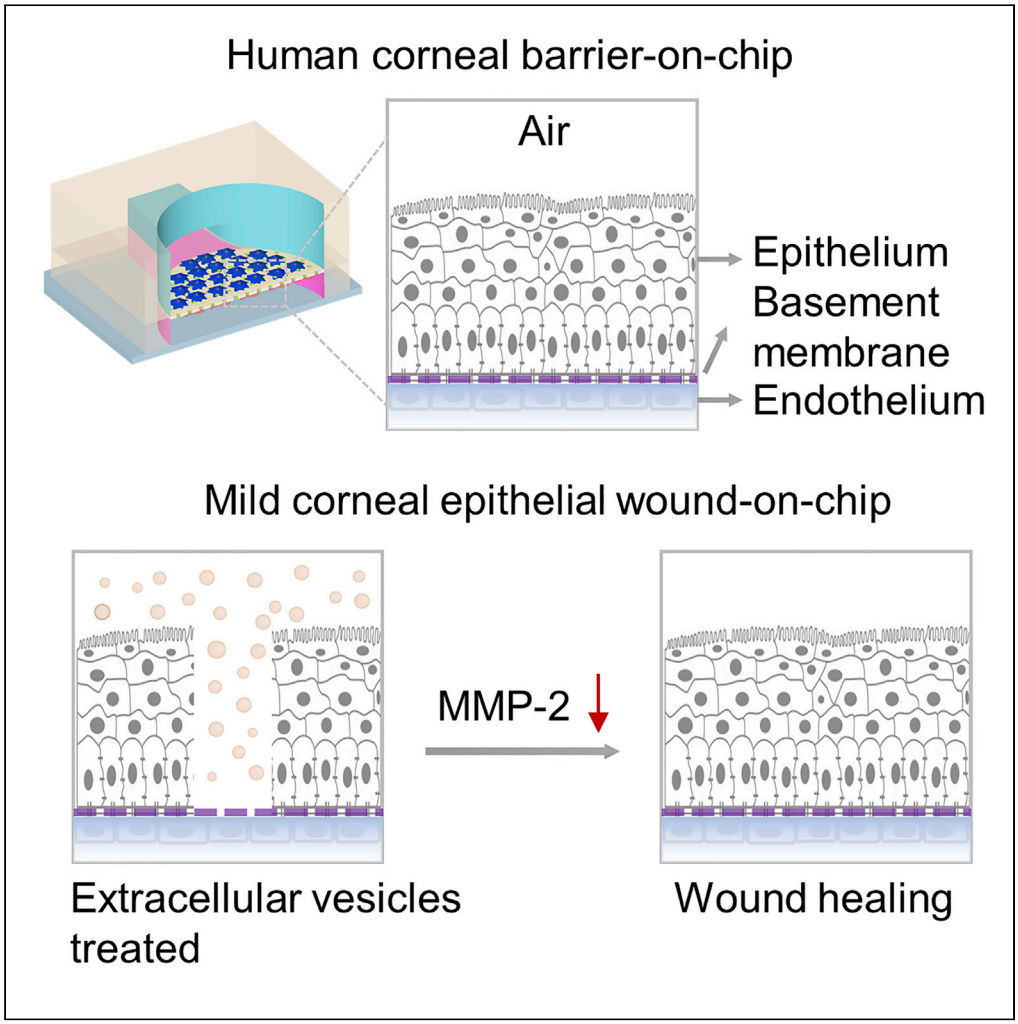

Zitong Yu, Rui Hao, Jing Du, ..., Wei Li, Zhongze Gu, Hui Yang

hui.yang@siat.ac.cn

Highlights

Combined human corneal cells and microfluidics to mimic ocular surface *in vitro*

Integrated human cornea's barrier effects on the microfluidic platform

In vitro model of mild corneal epithelial wound to test cell-free therapeutics

Extracellular vesicles accelerate corneal epithelial wound healing

Yu et al., iScience *25*, 104200
May 20, 2022
https://doi.org/10.1016/j.isci.2022.104200

iScience

CellPress
OPEN ACCESS

Article

A human cornea-on-a-chip for the study of epithelial wound healing by extracellular vesicles

Zitong Yu,[1] Rui Hao,[1] Jing Du,[1] Xiaoliang Wu,[1] Xi Chen,[1] Yi Zhang,[2] Wei Li,[3,4] Zhongze Gu,[5] and Hui Yang[1,6,*]

SUMMARY

Organs-on-chips are microfluidic devices for cell culturing to simulate tissue-level or organ-level physiology and recapitulate their microenvironment, providing new and significant solutions other than traditional animal tests. *In vitro* testing platforms for ocular biological studies have been increasingly used in preclinical efficacy and toxicity prediction. Here, we developed a microfluidic platform consisting of human corneal cells and porous membrane, replicating the multi-scale structural organization and biological phenotype. We verified the fully integrated human cornea's barrier effects on the chip. Moreover, we found that extracellular vesicles derived from bone marrow-derived mesenchymal stem cells can significantly accelerate the mild corneal epithelial wound healing, and the decreased expression of matrix metallopeptidase-2 protein indicated that this method effectively inhibits corneal inflammation and angiogenesis. This work improves our ability to simulate the interaction between the human cornea and the external world *in vitro* and contributes to the future development of new screening platforms for biopharmaceuticals.

INTRODUCTION

As exposed to the external environment, the human cornea is sensitive to environmental agents associated with eye damage (Ono et al., 2010) and vulnerable to traumatic injuries, such as corneal abrasions or chemical burns, which may damage the corneal barrier and even cause a loss of vision (Whitcher et al., 2001). Corneal wound healing has attracted academic researchers and clinical practitioners' great interest in understanding the corneal healing mechanism better and developing effective methods to improve wound healing (Bollag et al., 2020). Nowadays, most therapeutic studies on the cornea for ophthalmic applications are carried out with two-dimensional (2D) culture *in vitro*, three-dimensional (3D) culture *in vitro* or *ex vivo*, or with animal model conditions (Los, 2008; Xiong et al., 2008; Reichl et al., 2004). Although 2D culture models can provide large amounts of relatively low-cost data, they poorly represent complex pathophysiology in patients and hardly predict *in vivo* responses. The conventional trans-well 3D culture *in vitro* models can mimic physiological barrier function more accurately than the 2D models (Esch et al., 2015). However, they are usually performed under static conditions that are different from *in vivo* dynamic conditions, such as eyelid opening and tear film (Zieske, 2004). Although animal models can emulate physiological complexity at the organism level, there are always ethical issues. Studies have also shown the limited ability of these tests to recapitulate the human cornea's complex structure because of species differences. For example, the low blinking rate in rabbits can cause longer interaction between the drug and the ocular surface, resulting in higher drug permeation, which may mislead preclinical test results (Maurice, 1995).

In recent years, microphysiological systems have attracted much attention to establish standardized *in vitro* testing platforms for ophthalmology research. In a broader sense, microphysiological systems including organoid, 3D-printed tissue construct, and organ-on-a-chips are physiologically relevant *in vitro* models (Wang et al., 2020). Researchers have shown that complex 3D corneal organoids can be generated from the human-induced pluripotent stem cells and recapitulate corneal development steps (Foster et al., 2017). Alternatively, organ-on-a-chip technology relies on our knowledge of human organs to engineer man-made constructs in which cells and their microenvironment are precisely controlled. The optical transparency of organ-on-a-chip device is another significant advantage over animal models because it enables direct real-time visualization and high-resolution quantitative analysis of diverse biological processes (Li et al., 2013). Besides, the design of compartmentalized channels for cocultivation in organ-on-chips allows independent fluidic access to different tissue types within a single device and assures parametric control of

[1]Bionic Sensing and Intelligence Center, Institute of Biomedical and Health Engineering, Shenzhen Institutes of Advanced Technology, Chinese Academy of Sciences, Shenzhen 518055, China

[2]Center for Medical AI, Institute of Biomedical and Health Engineering, Shenzhen Institutes of Advanced Technology, Chinese Academy of Sciences, Shenzhen 518055, China

[3]Department of Ophthalmology, Xiang'an Hospital of Xiamen University, Xiamen 361102, China

[4]Fujian Provincial Key Laboratory of Ophthalmology and Visual Science, Eye Institute of Xiamen University, School of Medicine, Xiamen University, Xiamen 361102, China

[5]School of Biological Science and Medical Engineering, Southeast University, Nanjing 210096, China

[6]Lead contact

*Correspondence: hui.yang@siat.ac.cn

https://doi.org/10.1016/j.isci.2022.104200

microenvironmental factors (Esch et al., 2015). Microfluidic-based eye models that simulate eye events have been developed, such as corneal epithelium chips to evaluate eye drops, human blinking eye chips to study dry eye disease, and corneal barrier chips to emulate and evaluate an eye blinking shear force (Bennet et al., 2018; Seo et al., 2019; Abdalkader and Kamei, 2020). However, these models do not provide a complete human corneal structure, which is critical for recapitulating the micro-ocular physiological environment in corneal diseases and mass transport studies of ocular drugs.

The adult cornea consists of a stratified nonkeratinizing epithelial cell layer, a thick, highly aligned collagenous stroma interspersed with keratocytes, and a single cell-layered endothelium (Zieske, 2004). The epithelium sits atop a Bowman's layer, and the endothelial layer resides on a thickened basement membrane, termed Descemet's membrane (Zieske, 2004). This basement membrane consists of a felt-like arrangement of fibers, bumps, and pores with feature sizes in the nanometer to the submicron range, playing a major role in modulating cell behaviors such as proliferation, differentiation, and migration (LeBleu et al., 2007). Here, we designed a 3D *in vitro* ocular model using a membrane modified with extracellular matrix (ECM) to simulate the middle three layers and culturing corneal epithelial cells and endothelial cells on each side of the membrane to reproduce the physiological structure of the cornea. Then, the model was used to study corneal-related diseases and therapeutic methods further.

Corneal wounds caused by chemical or thermal burns, traumatic injury, immune disorders, and hereditary disorders are associated with inflammation, neovascularization, ulceration, and scarring (Whitcher et al., 2001). Improper or delayed treatment may lead to blindness (Thylefors, 1992). Therefore, it is highly desirable to discover methods to accelerate corneal wound healing to avoid the pain associated with corneal injuries and the possibility of infection because of barrier destruction. Together with embryonic stem cells/induced pluripotent stem cells (Taylor, 2016), non-retinal-derived adult stem cells—in particular neural stem cells and mesenchymal stem cells derived from bone marrow (BM-MSCs)—have been widely studied for eye therapies. MSCs with regeneration and differentiation capabilities have received much attention among ophthalmologists and visual scientists as an alternative modality in the management of corneal diseases (Taylor, 2016), and they can be useful sources of paracrine factors that protect retinal ganglion cells and stimulate regeneration of their axons in the optic nerve in degenerative eye diseases. However, it remains uncertain whether MSCs have long-term adverse effects on the immune system and whether there is a possibility of inducing tumorigenesis. On the other hand, the therapeutic effects of MSCs are widely mediated by MSCs differentiation and paracrine signaling via extracellular vesicles (EVs) (Burrello et al., 2016). The cell-free nature of EVs has gained particular interest concerning their safety on therapeutics (Mansoor et al., 2019). Thus, EVs derived from BM-MSCs could be of great potential for corneal wound healing.

Here, we present a human cornea-on-a-chip consisting of human epithelial and endothelial corneal cells as well as a collagen-coated porous membrane to mimic the Bowman's layer, stroma, and the Descemet's membrane. This microfluidic device integrated the compartmentalized channels for cocultivation to achieve the fully integrated human cornea on the chip and then used to evaluate EVs' efficacy for the corneal epithelial wound repair process. A porous membrane was used to separate the upper and lower channels that were designed for independent fluidic access to different cell types and parametric control of microenvironmental factors. Moreover, an open-top structure was constructed on the upper layer of the device made by polydimethylsiloxane (PDMS), providing a culture condition with an air-liquid interface (ALI) for the corneal epithelial cells, so physiological characteristics of the device are similar to the human cornea. The microfluidic device was then characterized and its functionality was verified by building and measuring the human cornea model in this study. In addition, the microfluidic chip was used to establish an *in vitro* mild corneal injury model to study whether cell-free therapy promotes corneal wound healing. We found that the EVs derived from BM-MSCs can significantly promote cell migration and also reduce the expression of matrix metallopeptidase 2 (MMP-2) protein, indicating that it can inhibit corneal inflammation and neovascularization, which is beneficial for wound healing. We demonstrated a micro-engineered device that improved the interaction between the *in vitro* model and external environments, providing a potential solution to obtain predictive results to *in vivo* observations.

RESULTS AND DISCUSSION

Cornea-chip design and fabrication

In general, the construction of any organ-on-a-chip system is guided by design principles based on a reductionist analysis of its target organ (Park et al., 2019). The first step is to understand the anatomy of

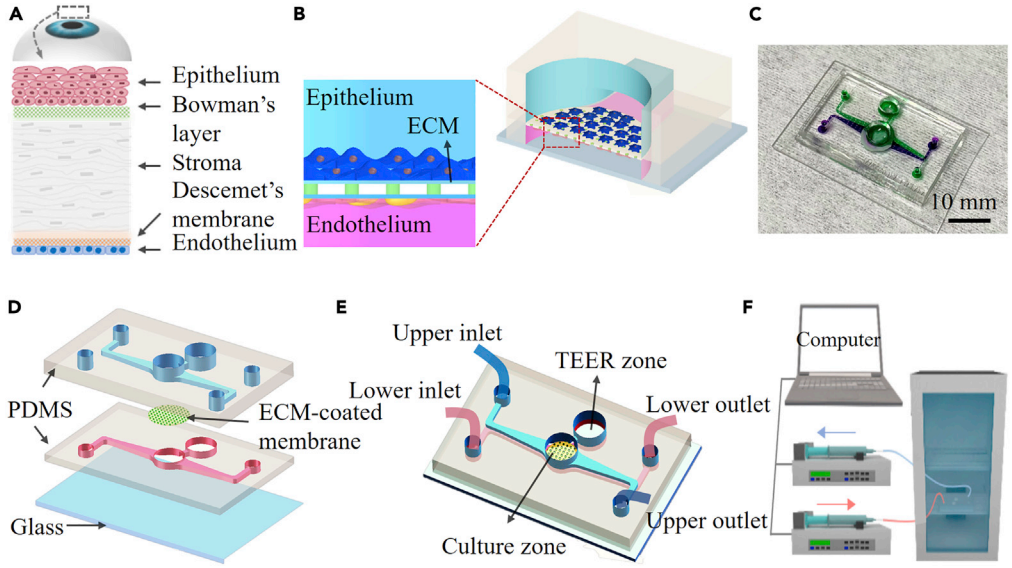

Figure 1. Schematic diagram of human cornea and design of the cornea-chip

(A) The anatomy of the human cornea.

(B) Cross-sectional schematic diagram of the corneal chip. HCEpi and HCEnd cells are cultured on the opposite sides of a porous PC membrane coated with ECM. The membrane is sandwiched between two PDMS layers incorporated with microfluidic channels.

(C) Photographs of the human cornea-chip; upper and lower microfluidic structures are indicated by using solutions with purple and green color dye.

(D) Three-dimensional illustration on the device, showing the details on the structures on different layers.

(E) The cornea-chip with two individual microfluidic channels and a circular hole in the middle mimics the human corneal structure. Structures for *in situ* TEER measurements are also fabricated on the chip.

(F) Experimental setup for flow control and cell culture. The device is located in an incubator with two microchannels connected to respective syringe pumps.

the target organ and reduce it to the basic elements essential for physiological function (Park et al., 2019). Cornea is the outermost organ structure of the eye. At the tissue level, cornea consists of epithelium, Bowman's layer, stroma, Descemet's membrane, and endothelium (Figure 1A). The cornea is a transparent avascular tissue that acts as a structural barrier and protects the eye against infections (DelMonte and Kim, 2011). The barrier function is one of the most important functions of the cornea (Mannermaa et al., 2006). There are tight cellular barriers, corneal epithelium and endothelium in the anterior and posterior parts of the eye that restrict the uptake of fluids and prevent penetration of foreign bodies (Sridhar, 2018). Hence, we selected human corneal epithelial and endothelial cells to establish the cornea's barrier *in vitro*. Next, the design principles define that a cell culture device should be designed to replicate the identified features (Park et al., 2019). Based on recognized materials and methods for constructing organ-on-chips (Huh et al., 2013; Brown et al., 2016; Zhang et al., 2012), we developed a biomimetic human corneal model on a microfluidic device with an integrated 0.4 μm porous polycarbonate (PC) membrane. In most organ-on-chips, PDMS structures have been widely used as substrates for cell culture and porous polymeric membranes as supporting layers to separate an apical and a basolateral compartment (Huh et al., 2010, 2012; Pasman et al., 2018). The interaction between cells and ECM proteins plays an important role in the regulation of cellular activities such as migration, proliferation, and differentiation (Juliano and Haskill, 1993). In the cornea, type I collagen, the major component of the corneal stroma, occupies the extracellular space and provides structural support to the keratocytes (Suzuki et al., 2003). Because ECM has been a crucial contributor in regulating cell functions *in vivo*, an ECM-coated membrane was used in our chip to promote cell attachment and differentiation (Fischer et al., 2012). The microfluidic device configuration was designed so that the upper and the lower microfluidic channels can be controlled independently. Therefore, human corneal epithelial (HCEpi) cells and human corneal endothelial (HCEnd) cells were seeded on the upper and lower side of the membrane, respectively (Figure 1B), and cultured in nutrients that were injected into different microchannels (Figure 1C). The barrier function is one of the most important functions of the cornea (Mannermaa et al., 2006). The open "Culture zone" provides the

necessary ALI condition for the differentiation of corneal epithelial cells into multilayer cells and form a natural barrier function, thereby simulating the physiological environment of the ocular surface more precisely.

The microfluidic device was fabricated by directly bonding a glass substrate with two PDMS layers sequentially and an ECM-coated PC membrane was sandwiched in between (Figure 1D). The upper and lower PDMS layers with microchannels were both replicated from SU-8 structures fabricated by soft lithography. A 10:1 (w/w) mixture of PDMS prepolymer and curing agent was cast over the SU-8 molds and cured at 80°C overnight. The PDMS replicas were peeled off from the molds, resulting in microfluidic channels with a height of 220 μm. Access holes for inlets and outlets of the microfluidic channels were punched on the PDMS slabs. At the middle of the microfluidic channel, a circular hole with diameter of 6 mm was punched on each PDMS slab. This hole was used to mimic the human corneal structure, and the open-top surface of this area was used to create an air-liquid interface and mimic the ocular surface more precisely. By thoroughly cleaning the glass substrate and the PDMS layers, they were bonded together by oxygen plasma with the PC membrane embedded between the two microfluidic channels. Trans-epithelial electrical resistance (TEER), an acknowledged method for evaluating corneal barrier function *in vitro*, can be measured *in situ* through the "TEER zone" that was made on the device and connected to the cell culture area (Figure 1E) (Shafaie et al., 2016).

More details on the microfabrication procedure are presented in the Supporting Information in Figure S1. Scanning electron microscopy (SEM) images showing the cross-section of the device are shown in Figure S2.

Recapitulating physiological phenotypes of the human cornea

Before the surface treatment, the chip was sterilized by UV germicidal irradiation in a biosafety cabinet for 30 min. Then, collagen (0.05 mg/mL in 0.02 M acetic acid) was used as the ECM to treat the PC membrane (Bennet et al., 2018; Newsome et al., 1981). The device was injected with a 100 μL of ECM solution to let it incubate on the PC membrane at 37°C for 2 h. Excess proteins were then aspirated and the membrane was allowed to air dry. HCEpi cells and HCEnd cells were introduced into the device at initial densities of 3×10^6 cells/mL and 5×10^5 cells/mL through the upper and lower microchannels, respectively. Thereafter, 6×10^4 HCEpi cells and 1×10^4 HCEnd cells were then seeded on each side of the membrane and cultured with their medium at a continuous flow condition with a volumetric flow rate of 100 μL/h by using a programmable low-pressure syringe pump (Cetoni neMESYS). The device was kept in a CO_2 incubator (Figure 1F). Once the epithelial layer was confluent on the membrane, the culture medium was gently aspirated from the 6 mm hole at the middle of the upper microfluidic channel, and air was then filled the epithelial compartment to create an air-liquid interface and mimic the ocular surface. TEER values were measured *in situ* using a Millicell-ERS electrical resistance system on different days to evaluate the corneal epithelium's barrier integrity. After 7 and 14 days, the cornea chip was characterized using immunofluorescence staining and monitored by a Zeiss Axio Observer 7 inverted fluorescence microscope equipped with light-emitting diodes, appropriate fluorescent filter sets, and an sCMOS camera.

To mimic the ocular surface more precisely and optimize the culture conditions of the human corneal cells, HCEpi cells were grown on chip either with an immersed condition ("Chip (Epi-immersed)") or with an air-liquid interface condition ("Chip (Epi-ALI)"). At the early stage of the experiments, the HCEpi cells were also cultured in transwell inserts ("Transwell (Epi-ALI)") as a comparison. The human corneal cells were maintained in these groups for up to 14 days to investigate whether the microfluidic chip was suitable for human corneal cell culture. The H&E staining results show that the PC membrane with 0.4 μm pore size contributes to the proliferation and differentiation of multilayered cells in the corneal epithelium ("Transwell (Epi-ALI)" in Figure 2A). Therefore, the same membrane was used on the chip for cell cultivation. In addition, the HCEpi cells cultured with the air-liquid interface condition formed a stratified epithelium consisting of five to seven stacked cell layers (about 23.1 μm in thickness), which recapitulated the corneal epithelium *in vivo* ("Chip (Epi-ALI)" in Figure 2A). However, the thickness of stratified corneal epithelium formed by HCEpi cells that were cultured with the immersed condition ("Chip (Epi-immersed)" in Figure 2A) was 13.5 μm, indicating that the immersed condition was not suitable for culturing the HCEpi cells on chip.

Moreover, the TEER value was measured to evaluate barrier integrity after culturing HCEpi cells on a transwell model or on chip for 3, 7, 10, and 14 days (Figure 2B). The measurement results were presented as $\Omega \cdot cm^2$ by multiplying the resistance with the surface area, which is 0.28 cm^2 for the open well on the microfluidic device. The resistance of the unseeded cell membrane was subtracted from all readings before calculations. The human

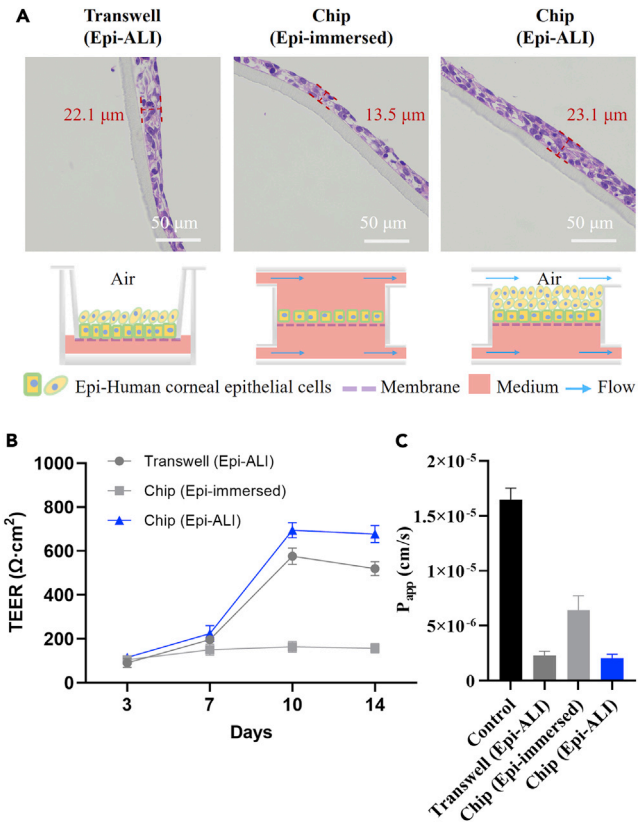

Figure 2. Optimization on the culture conditions of HCEpi cells

(A) H&E images on the stratified corneal epithelium in different conditions after 14 days. "Transwell (Epi-ALI)" group acts as the positive control. "Chip (Epi-immersed)" and "Chip (Epi-ALI)" represent HCEpi cells grown either with the immersed condition or with an air-liquid interface (ALI) condition, respectively. Red dotted lines and numbers indicate the thickness of the stratified corneal epithelium.

(B) TEER values of the corneal epithelium that are measured at 3, 7, 10, and 14 days, respectively.

(C) Measurement of corneal epithelium permeability coefficient (Papp) by using 5 kDa FITC-Dextran. Control means the membrane without cells. (B) (C) All data are mean ± SD from three independent experiments.

corneal epithelium began to form a barrier function when the cells were cultured for 3 days. The air-liquid interface condition is critical for the HCEpi cells to form an integrated barrier. The measurement result shows that the TEER value of the cells cultured in the immersed condition does not increase after 7 days, unlike that of the cells cultured with the air-liquid interface condition. Moreover, after being cultured for 10 days, the barrier function obtained from the cornea-chip is higher than that from the transwell model. Therefore, our device was suitable for HCEpi cells culture, especially with the air-liquid interface to mimic their native organ-specific environment. Besides, the apparent permeability index (Papp) is the index used to assess the permeability of substances (Newsome et al., 1981; Ravikanth and Ramanamurthy, 2018). In former studies, Huang and coworkers found that the whole cornea with intact epithelium, stroma, and endothelium was permeable only to mannitol (molecular weight (MW) 182) but not inulin (MW 5000) (Huang et al., 1989). Generally, the Papp index lower than 2×10^{-6} cm/s indicates low permeability. Although the Papp result of the "Chip (Epi-ALI)" group (2.06×10^{-6} cm/s) was lower than all the other groups (Figure 2C), FITC-Dextran with an average MW of 3000–5000 can still penetrate the barrier, indicating that the *in vitro* model constructed by a single type of corneal cells, i.e., the HCEpi cells, would hardly achieve the low permeability similar to the physiological environment. To construct a whole cornea, we cocultured the HCEpi and HCEnd cells on our device and further investigated the barrier integrity.

The cell viability of the human corneal cells, i.e., HCEpi and HCEnd cells cocultured on chip, was evaluated using a Calcein-AM/PI double stain kit and Cell Counting Kit-8 (CCK-8) assay, respectively. The CCK-8 assay results showed that both HCEpi cells and HCEnd cells proliferated stably for 72 h, indicating their

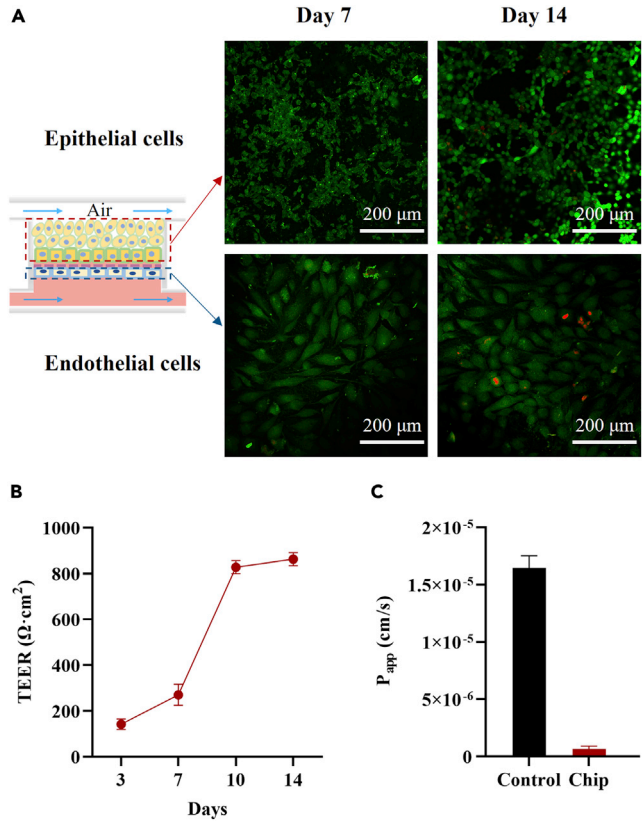

Figure 3. Construction of biomimetic coculture platform of the human corneal cells in the microfluidic chip

(A) Microscopy images on the cell viability of the HCEpi cells and the HCEnd cells cocultivated in the cornea-chip. Cells are treated by Calcein-AM (live cells, green color) and PI (dead cells, red color) before observation.

(B) TEER values obtained from the cornea-chip at 3, 7, 10, and 14 days.

(C) Measurement of the corneal permeability coefficient (Papp) on 5 kDa FITC-Dextran. (B) (C) All data are mean ± SD from three independent experiments.

good cell viability. More details are provided in the Supporting Information (Figure S3). Although it is challenging for the HCEnd cells to proliferate *in vitro*, their morphology was still good after long-term culture, because the condition in our chip is similar to the physiological condition of the ocular surface (see Figure 3A). The TEER values of the cocultured chip kept increasing with time (about 862 Ω cm^2 at 14 days), and the Papp result of the "Chip" group was 6.63 × 10^{-7} cm/s with low permeability, indicating that the cocultivation was more conducive to the formation of the corneal tissue (see Figures 3B–3C).

Prolonged ALI culture led to substantial morphological and biochemical changes indicative of cell differentiation. These morphological changes were accompanied by the expression of cytokeratin-3 (Figure S4A), which are specific to terminally differentiated corneal epithelial cells (Reynolds et al., 1999). In addition, the differentiated cells formed tight junctions (Figure S4B) and microscopic protrusions on their apical surface were identical to microvilli and microprojections on the human cornea (Versura et al., 1985) (Figure S4C). More details are provided in the Supporting Information (Section S4).

The epithelial and endothelial tight junctional barrier plays a crucial role in homeostasis and host defense of the cornea (Yin and Watsky, 2005). The expression of tight junction proteins can reflect the barrier function. A substantial increase in the expression of zona occludens-1 (ZO-1) protein accompanies the full barrier function. Further experiments were performed to discuss the difference on ZO-1 protein expression obtained from the microfluidic chip either by culturing a single type of human corneal cells ("Epi only" in Figure 4A or "End only" in Figure 4C) or by coculturing these two kinds of cells ("Chip" in Figures 4A and 4C). The cell morphology and the expression of ZO-1 of HCEnd and HCEpi cells are shown in Figures 4A and 4C. After 14 days, the cells' morphology remained very well, and the expression of ZO-1 was significantly increased in the experimental

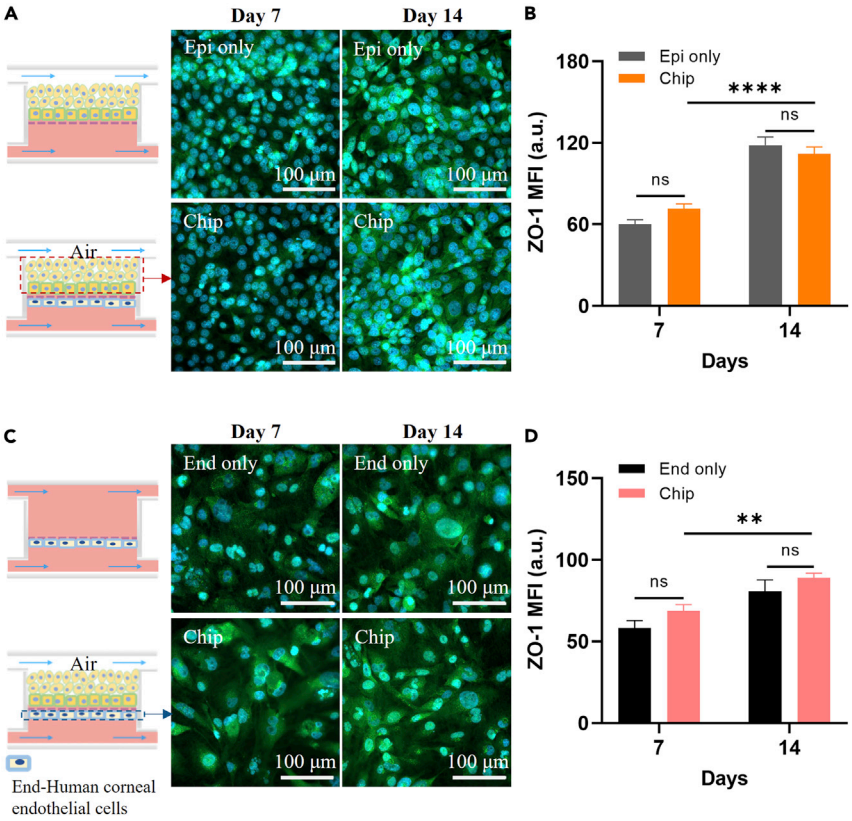

Figure 4. Construction of physiological phenotypes of the human cornea

(A and C) Immunofluorescent characterization of human corneal cells cultured in different conditions. "Epi only" or "End only" represents a single type of cells cultured in the chip, respectively. "Chip" means the coculture of the HCEpi cells and HCEnd cells. The green color is the immunofluorescence staining of ZO-1 protein, and the blue color shows the cell nucleus by DAPI staining.

(B) Mean fluorescent intensity (MFI) of ZO-1 protein expression obtained from Figure 4A.

(D) MFI of ZO-1 protein expression obtained from Figure 4C a.u., arbitrary unit. (B and D) Data are mean ± SD of relative fluorescence intensity from three independent experiments. P values by two-way ANOVA and Bonferroni's multiple comparisons test. "ns" no significant difference, "**" $p < 0.01$, "****" $p < 0.001$.

groups (Figures 4B and 4D). Besides, the ZO-1 expression kept increasing with time. Compared to the "Chip", the ZO-1 expression of the "Epi only" was a little bit higher on the 14th day. After 14 days, the intact human corneal tissues have been formed on the chip, and the contact inhibition between the tissues may occur, leading to a decreased ZO-1 expression. It was found that contact inhibition is an important mechanism responsible for inducing cell-cycle arrest during corneal endothelial development and maintaining the mature monolayer in a no proliferative state (Joyce et al., 2002).

In vitro mild corneal scratch wound healing model

Extracellular vesicles (EVs) are heterogeneous, membrane-bound phospholipid vesicles with a diameter of about 30–200 nm, and they originate from the fusion of intracellular multivesicular bodies with the cell membrane and are released into the extracellular spaces (Shao et al., 2018). The EVs have been reported for many biological and medical applications, such as treating cardiovascular disease (Lai et al., 2011), ameliorating renal oxidative stress (Zhou et al., 2013), suppressing VEGF expression in breast cancer cells, and promoting corneal epithelial wound healing (Lee et al., 2013; Samaeekia et al., 2018). It has been reported that EVs derived from MSC cells are most effective in stimulating cell proliferation. Therefore, MSC-EVs have been widely studied for applications such as cell-free therapy (Mansoor et al., 2019).

Corneal wounds caused by various chemical, physical, and pathological insults damage the corneal epithelium, resulting in disruption of its barrier function, wound formation, and may even cause loss of vision

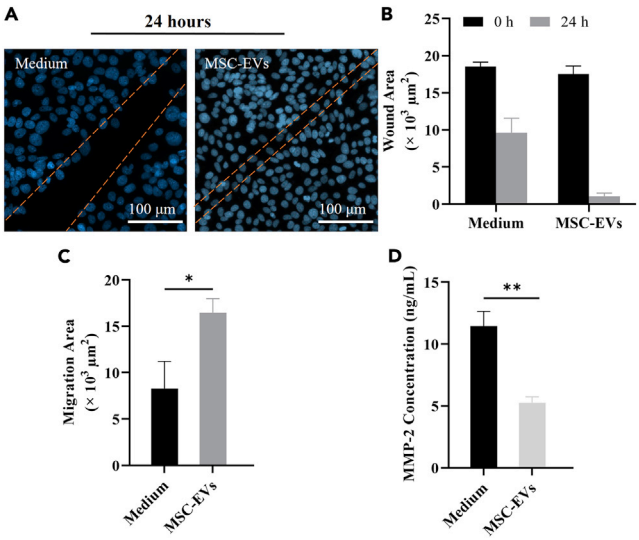

Figure 5. EVs derived from MSCs cells stimulate scratch wound healing of immortalized HCEpi cells on-chip

(A) Micrographs showing wound closure at 24 h from different experimental conditions. The cells are treated by serum-free cell culture medium ("Medium"), and EVs are derived from MSCs ("MSC-EVs"). The approximate wound edges are indicated with orange lines. The blue color shows the cell nucleus by DAPI staining.

(B) Wound areas at 0 h and 24 h.

(C) Migration areas after 24 h.

(D) ELISA results of the MMP-2 expression from different treatment groups. (B) (C) (D) All data are mean ± SD from three independent experiments. P values by two-way ANOVA and Bonferroni's multiple comparisons test. "*" $p < 0.05$, "**" $p < 0.01$.

(Ljubimov and Saghizadeh, 2015). Therefore, it is highly desirable to discover methods to accelerate corneal wound healing to avoid the pain associated with corneal injuries and the possibility of infection because of barrier destruction. The corneal wound healing response is typically initiated by injuries to the epithelium and/or endothelium that may also involve the stroma (Wilson, 2020). For mild injuries or infections such as epithelial abrasions or mild controlled microbial infections, limited keratocyte apoptosis occurs, the epithelium or endothelium regenerates, and the epithelial basement membrane and/or Descemet's basement membrane is repaired (Wilson, 2020). For more severe injuries with extensive damage to epithelial basement membrane and/or Descemet's basement membrane, delayed regeneration of the basement membranes leads to ongoing penetration of the pro-fibrotic cytokines transforming growth factor (TGF) β1, TGFβ2, and platelet-derived growth factor (PDGF) that drive the development of mature alpha-smooth muscle actin (SMA)+ myofibroblasts that secrete large amounts of disordered ECM components to produce scarring stromal fibrosis (Wilson, 2020). Fibrosis is dynamic with ongoing mitosis and development of SMA + myofibroblasts and continued autocrine-or paracrine interleukin (IL)-1-mediated apoptosis of myofibroblasts and their precursors (Wilson, 2020). Eventual repair of the epithelial basement membrane and/or Descemet's basement membrane can lead to at least partial resolution of scarring fibrosis (Wilson, 2020). Therefore, our model built on the chip can be a good solution to study mild corneal injuries.

We investigated the mild corneal epithelial cell scratch wound healing *in vitro* on the microfluidic chip using EVs isolated from the cell culture medium of MSCs. The mild scratch wound was made by a pipet tip on the epithelial layer, and then treated by serum-free cell culture medium as the control group and 1×10^8 MSC-EVs/mL, respectively. More details on the amount of MSC-EVs are provided in the Supporting Information (Figure S7). The healing of corneal epithelial wounds involves a number of concerted events including cell migration, proliferation, adhesion, and differentiation with cell layer stratification (Ljubimov and Saghizadeh, 2015). The first phase of epithelial wound healing is characterized by epithelial migration in which the adhesion of epithelial cells to the ECM plays a prominent role (Suzuki et al., 2003). Cell-cell adhesion is also an important factor in corneal epithelial wound healing (Suzuki et al., 2003). The representative wound edges at 24 h are indicated with orange lines in Figure 5A. The area between the leading edges of the wound was determined at time 0 and subtracted from the wound area at 24 h to obtain a value

for the wound size difference (see Figure 5B). Compared to the "Medium" group, the MSC-EVs group enhanced cell migration by approximately 1.9-fold (Figure 5C), demonstrating that the MSC-EVs contribute tremendously to cell migration.

It has been reported that, under the injured condition, the transplanted MSCs could produce a set of signaling effectors that result in a decrease of host pro-inflammatory cytokines, e.g., MMP-2, and an increase of anti-inflammatory cytokine, e.g., IL-6, and growth factor, e.g., TGFβ. These factors then initiate the downstream signaling transduction and finally repress inflammation. Moreover, MSCs also change the levels of many angiogenesis-associated factors in the cornea, such as MMP-2 and VEGF, which reduce neovascularization (Oh et al., 2008). We, therefore, quantitated the MMP-2 expression to verify the effectiveness of different treatments for scratch wound healing. The expression of MMP-2 protein was quantitated with a human MMP-2 ELISA kit according to the manufacturer's protocols. More details on the MMP-2 standard curve are provided in the Supporting Information (Figure S8). The device unseeded with cells and treated by serum-free culture medium was performed as the control group, and the data was subtracted from all readings before being analyzed. The MMP-2 ELISA results showed that the treatment with MSC-EVs was the lowest, indicating that they have the effect of inhibiting corneal inflammation and neovascularization (Figure 5D).

CONCLUSIONS

In this study, we developed a human cornea-on-a-chip using microfluidic technology, validated its barrier effects, and tested a cell-free therapeutic method to heal a scratch wound using MSC-EVs. In brief, the cornea-chip has a complete human corneal structure, and its physiological characteristics are much closer to that of the human cornea, so its suitability for the applications such as corneal disease study, evaluation of ocular drug absorption and permeation, as well as emulation of tissue barrier function can be envisaged in future. This corneal chip may replace animal models for cornea-related testing, which will provide meaningful, predictive, and complimentary results to *in vivo* and *ex vivo* observations. Therefore, we believe that our technique could evolve into a tool for a comprehensive class of biological and clinical applications.

Limitations of the study

This study is only the starting point of a fully functionalized human cornea-chip platform and its comprehensive applications *in vitro*. One limitation is that the cornea-chip relies on a programmable syringe pump to recapitulate the microenvironment *in vivo*, which depends on an external device during the coculture process and limits the system flexibility. In addition, the corneal wound healing response is typically initiated by injuries to the epithelium and/or endothelium that may also involve the stroma (Wilson, 2020). For mild injuries or infections, such as epithelial abrasions or mild controlled microbial infections, limited keratocyte apoptosis occurs, the epithelium or endothelium regenerates, and the epithelial basement membrane and/or Descemet's basement membrane is repaired (Wilson, 2020). For more severe injuries with extensive damage to epithelial basement membrane and/or Descemet's basement membrane, the stroma layer also plays an important role in wound repair. IL-1α is released from the injured epithelium into the stroma and induces some of the underlying stromal keratocytes to undergo cell death, whereas others are induced to proliferate, secrete MMPs, and transit from a quiescent to an activated phenotype (Wilson, 2020). The return of the basement membrane inhibits the release of TGFβ2 into the stroma and the activated keratocytes continue to secrete autocrine IL-1α and remodel the ECM (Wilson, 2020). Eventual repair of the epithelial basement membrane and/or Descemet's basement membrane can lead to at least partial resolution of scarring fibrosis (Wilson, 2020). Therefore, our chip is suitable for studying mild injuries or infections. However, for more severe injuries, the model needs to be optimized. Moreover, the mechanism of MSC-EVs on human corneal wound healing remains unknown in this study and requires further investigation.

STAR★METHODS

Detailed methods are provided in the online version of this paper and include the following:

- KEY RESOURCES TABLE
- RESOURCE AVAILABILITY
  - Lead contact
  - Materials availability
  - Data and code availability
- EXPERIMENTAL MODEL AND SUBJECT DETAILS

SUPPLEMENTAL INFORMATION

Supplemental information can be found online at https://doi.org/10.1016/j.isci.2022.104200.

ACKNOWLEDGMENTS

We acknowledge financial support from Key Area Research and Development Program of Guangdong Province (2019B020226004), Guangdong Program (2016ZT06D631), National Natural Science Foundation of China (NSFC, No. 62074155, 62175252), and Shenzhen Science and Technology Innovation Commission (KZXFZ202002011008124).

AUTHOR CONTRIBUTIONS

H.Y. and Y.Z. conceived the study. H.Y. supervised the project. Z.Y. and H.Y. designed the experiments. Z.Y., R.H., J.D., X.W., and X.C. performed the experiments. Z.Y., R.H., and H.Y. wrote the manuscript. W.L., Z.G., and H.Y. supervised and edited the manuscripts.

DECLARATION OF INTERESTS

The authors declare no competing interests.

Received: August 2, 2021
Revised: January 27, 2022
Accepted: April 1, 2022
Published: May 20, 2022

REFERENCES

Abdalkader, R., and Kamei, K.I. (2020). Multi-corneal barrier-on-a-chip to recapitulate eye blinking shear stress forces. Lab Chip *20*, 1410–1417.

Bennet, D., Estlack, Z., Reid, T., and Kim, J. (2018). A microengineered human corneal epithelium-on-a-chip for eye drops mass transport evaluation. Lab Chip *18*, 1539–1551.

Bollag, W.B., Olala, L.O., Xie, D., Lu, X., Qin, H., Choudhary, V., Patel, R., Bogorad, D., Estes, A., and Watsky, M. (2020). Dioleoylphosphatidylglycerol accelerates corneal epithelial wound healing. Invest. Ophthalmol. Vis. Sci. *61*, 29.

Brown, J.A., Codreanu, S.G., Shi, M., Sherrod, S.D., Markov, D.A., Neely, M.D., Britt, C.M., Hoilett, O.S., Reiserer, R.S., Samson, P.C., et al. (2016). Metabolic consequences of inflammatory disruption of the blood-brain barrier in an organ-on-chip model of the human neurovascular unit. J. Neuroinflammation *13*, 306–317.

Burrello, J., Monticone, S., Gai, C., Gomez, Y., Kholia, S., and Camussi, G. (2016). Stem cell-derived extracellular vesicles and immune-modulation. Front. Cell Dev. Biol. *4*, 83.

DelMonte, D.W., and Kim, T. (2011). Anatomy and physiology of the cornea. J. Cataract Refract. Surg. *37*, 588–598.

Esch, E.W., Bahinski, A., and Huh, D. (2015). Organs-on-chips at the frontiers of drug discovery. Nat. Rev. Drug Discov. *14*, 248–260.

Fischer, R.S., Myers, K.A., Gardel, M.L., and Waterman, C.M. (2012). Stiffness-controlled three-dimensional extracellular matrices for high-resolution imaging of cell behavior. Nat. Protoc. *7*, 2056–2066.

Foster, J.W., Wahlin, K., Adams, S.M., Birk, D.E., Zack, D.J., and Chakravarti, S. (2017). Cornea organoids from human induced pluripotent stem cells. Sci. Rep. *7*, 41286–41288.

Huang, A.J., Tseng, S.C., and Kenyon, K.R. (1989). Paracellular permeability of corneal and conjunctival epithelia. Invest. Ophthalmol. Vis. Sci. *30*, 684–689.

Huh, D., Kim, H.J., Fraser, J.P., Shea, D.E., Khan, M., Bahinski, A., Hamilton, G.A., and Ingber, D.E. (2013). Microfabrication of human organs-on-chips. Nat. Protoc. *8*, 2135–2157.

Huh, D., Leslie, D.C., Matthews, B.D., Fraser, J.P., Jurek, S., Hamilton, G.A., Thorneloe, K.S., McAlexander, M.A., and Ingber, D.E. (2012). A human disease model of drug toxicity-induced pulmonary edema in a lung-on-a-chip microdevice. Sci. Transl. Med. *4*, 159ra147.

Huh, D., Matthews, B.D., Mammoto, A., Montoya-Zavala, M., Hsin, H.Y., and Ingber, D.E. (2010). Reconstituting organ-level lung functions on a chip. Science *328*, 1662–1668.

Joyce, N.C., Harris, D.L., and Mello, D.M. (2002). Mechanisms of mitotic inhibition in corneal endothelium: contact inhibition and TGF-beta2. Invest. Ophthalmol. Vis. Sci. *43*, 2152–2159.

Juliano, R.L., and Haskill, S. (1993). Signal transduction from the extracellular matrix. J. Cell Biol. *120*, 577–585.

Lai, R.C., Chen, T.S., and Lim, S.K. (2011). Mesenchymal stem cell exosome: a novel stem cell-based therapy for cardiovascular disease. Regen. Med. *6*, 481–492.

LeBleu, V.S., MacDonald, B., and Kalluri, R. (2007). Structure and function of basement membranes. Exp. Biol. Med. (Maywood) *232*, 1121–1129.

Lee, J.K., Park, S.R., Jung, B.K., Jeon, Y.K., Lee, Y.S., Kim, M.K., Kim, Y.G., Jang, J.Y., and Kim, C.W. (2013). Exosomes derived from mesenchymal stem cells suppress angiogenesis

by down-regulating VEGF expression in breast cancer cells. PLoS One *8*, e84256.

Li, F., Yin, Z., Jin, G., Zhao, H., and Wong, S.T. (2013). Chapter 17: bioimage informatics for systems pharmacology. PLoS Comput. Biol. *9*, e1003043.

Ljubimov, A.V., and Saghizadeh, M. (2015). Progress in corneal wound healing. Prog. Retin. Eye Res. *49*, 17–45.

Los, L.I. (2008). The rabbit as an animal model for post-natal vitreous matrix differentiation and degeneration. Eye (Lond) *22*, 1223–1232.

Mannermaa, E., Vellonen, K.S., and Urtti, A. (2006). Drug transport in corneal epithelium and blood-retina barrier: emerging role of transporters in ocular pharmacokinetics. Adv. Drug Deliv. Rev. *58*, 1136–1163.

Mansoor, H., Ong, H.S., Riau, A.K., Stanzel, T.P., Mehta, J.S., and Yam, G.H. (2019). Current trends and future perspective of mesenchymal stem cells and exosomes in corneal diseases. Int. J. Mol. Sci. *20*, 2853.

Maurice, D. (1995). The effect of the low blink rate in rabbits on topical drug penetration. J. Ocul. Pharmacol. Ther. *11*, 297–304.

Newsome, D.A., Foidart, J.M., Hassell, J.R., Krachmer, J.H., Rodrigues, M.M., and Katz, S.I. (1981). Detection of specific collagen types in normal and keratoconus corneas. Invest. Ophthalmol. Vis. Sci. *20*, 738–750.

Oh, J.Y., Kim, M.K., Shin, M.S., Lee, H.J., Ko, J.H., Wee, W.R., and Lee, J.H. (2008). The anti-inflammatory and anti-angiogenic role of mesenchymal stem cells in corneal wound healing following chemical injury. Stem Cells *26*, 1047–1055.

Ono, K., Hiratsuka, Y., and Murakami, A. (2010). Global inequality in eye health: country-level analysis from the Global Burden of Disease Study. Am. J. Public Health *100*, 1784–1788.

Park, S.E., Georgescu, A., and Huh, D. (2019). Organoids-on-a-chip. Science *364*, 960–965.

Pasman, T., Grijpma, D., Stamatialis, D., and Poot, A. (2018). Flat and microstructured polymeric membranes in organs-on-chips. J. R. Soc. Interf. *15*, 20180351.

Ravikanth, P., and Ramanamurthy, K. (2018). Permeability assessment of drug substances using in vitro and ex vivo screening techniques. Innov. Pharm. Pharmacother. *6*, 17–20.

Reichl, S., Bednarz, J., and Müller-Goymann, C.C. (2004). Human corneal equivalent as cell culture model for in vitro drug permeation studies. Br. J. Ophthalmol. *88*, 560–565.

Reynolds, I., Tullo, A.B., John, S.L., Holt, P.J., and Hillarby, M.C. (1999). Corneal epithelial-specific cytokeratin 3 is an autoantigen in Wegener's granulomatosis-associated peripheral ulcerative keratitis. Invest. Ophthalmol. Vis. Sci. *40*, 2147–2151.

Samaeekia, R., Rabiee, B., Putra, I., Shen, X., Park, Y.J., Hematti, P., Eslani, M., and Djalilian, A.R. (2018). Effect of human corneal mesenchymal stromal cell-derived exosomes on corneal epithelial wound healing. Invest. Ophthalmol. Vis. Sci. *59*, 5194–5200.

Seo, J., Byun, W.Y., Alisafaei, F., Georgescu, A., Yi, Y.S., Massaro-Giordano, M., Shenoy, V.B., Lee, V., Bunya, V.Y., and Huh, D. (2019). Multiscale reverse engineering of the human ocular surface. Nat. Med. *25*, 1310–1318.

Shafaie, S., Hutter, V., Cook, M.T., Brown, M.B., and Chau, D.Y. (2016). In vitro cell models for ophthalmic drug development applications. BioResearch Open Access *5*, 94–108.

Shao, H., Im, H., Castro, C.M., Breakefield, X., Weissleder, R., and Lee, H. (2018). New technologies for analysis of extracellular vesicles. Chem. Rev. *118*, 1917–1950.

Sridhar, M.S. (2018). Anatomy of cornea and ocular surface. Indian J. Ophthalmol. *66*, 190–194.

Suzuki, K., Saito, J., Yanai, R., Yamada, N., Chikama, T., Seki, K., and Nishida, T. (2003). Cell-matrix and cell-cell interactions during corneal epithelial wound healing. Prog. Retin. Eye Res. *22*, 113–133.

Taylor, A.W. (2016). Ocular immune privilege and transplantation. Front. Immunol. *7*, 37.

Thylefors, B. (1992). Epidemiological patterns of ocular trauma. Aust. N. Z. J. Ophthalmol. *20*, 95–98.

Versura, P., Bonvicini, F., Caramazza, R., and Laschi, R. (1985). Scanning electron microscopy of normal human corneal epithelium obtained by scraping-off in vivo. Acta Ophthalmol. (Copenh) *63*, 361–365.

Wang, K., Man, K., Liu, J., Liu, Y., Chen, Q., Zhou, Y., and Yang, Y. (2020). Microphysiological systems: design, fabrication, and applications. ACS Biomater. Sci. Eng. *6*, 3231–3257.

Whitcher, J.P., Srinivasan, M., and Upadhyay, M.P. (2001). Corneal blindness: a global perspective. Bull. World Health Organ. *79*, 214–221.

Wilson, S.E. (2020). Corneal wound healing. Exp. Eye Res. *197*, 108089.

Xiong, C., Chen, D., Liu, J., Liu, B., Li, N., Zhou, Y., Liang, X., Ma, P., Ye, C., Ge, J., and Wang, Z. (2008). A rabbit dry eye model induced by topical medication of a preservative benzalkonium chloride. Invest. Ophthalmol. Vis. Sci. *49*, 1850–1856.

Yin, F., and Watsky, M.A. (2005). LPA and S1P increase corneal epithelial and endothelial cell transcellular resistance. Invest. Ophthalmol. Vis. Sci. *46*, 1927–1933.

Zhang, Q., Liu, T., and Qin, J. (2012). A microfluidic-based device for study of transendothelial invasion of tumor aggregates in realtime. Lab Chip *12*, 2837–2842.

Zhou, Y., Xu, H., Xu, W., Wang, B., Wu, H., Tao, Y., Zhang, B., Wang, M., Mao, F., Yan, Y., et al. (2013). Exosomes released by human umbilical cord mesenchymal stem cells protect against cisplatin-induced renal oxidative stress and apoptosis in vivo and in vitro. Stem Cell Res. Ther. *4*, 1–13.

Zieske, J.D. (2004). Corneal development associated with eyelid opening. Int. J. Dev. Biol. *48*, 903–911.

STAR★METHODS

KEY RESOURCES TABLE

REAGENT or RESOURCE	SOURCE	IDENTIFIER
Antibodies		
Anti-ZO1 tight junction protein rabbit polyclonal	Servicebio	Cat# GB111402; RRID:AB_2910249
Anti-MMP2 rabbit polyclonal	Servicebio	Cat# GB11130; RRID:AB_2910250
Anti-Cytokeratin 3/CK-3 mouse monoclonal	Abcam	Abcam Cat# ab68260; RRID:AB_1140695
Cy3 conjugated Goat Anti-Rabbit IgG (H + L)	Servicebio	Cat# GB21303; RRID:AB_2861435
FITC conjugated Goat Anti-Rabbit IgG (H + L)	Servicebio	Cat# GB22303; RRID:AB_2904189
Cy5 conjugated Goat Anti-Mouse IgG (H + L)	Servicebio	GB27301; RRID:AB_2910251
Chemicals, peptides, and recombinant proteins		
Polydimethylsiloxane	DOWCORNING	SYLGARDTM 184
SU-8	MicroChem	2100
Fetal bovine serum	Gibco	10099–141C
Human EGF	Peprotech	AF-100-15-100
Penicillin-streptomycin	Hyclone	SV30010
Recombinant human insulin	Applied Biological Materials Inc.	Z101065
Transferrin human	Sigma-Aldrich	T8158
Sodium selenite	Sigma-Aldrich	S5261
Hydrocortisone	Selleck Chemicals	S1696
β-estradiol	Sigma-Aldrich	E2758
Recombinant human VEGF (165aa)	Applied Biological Materials Inc.	Z100895
Heparin sodium	Selleck Chemicals	S1346
L-glutamine	Applied Biological Materials Inc.	G275
Collagen I, Rat Tail	Corning Inc.	354249
Paraformaldehyde	Sangon	E672002-0100l
Hematoxylin	Servicebio	G1005-1
Eosin	Servicebio	G1005-2
4′,6′-diamidino-2-phenylindole hydrochloride	Invitrogen	D1306
Fluorescein isothiocyanate–dextran (average MW 3000–5000)	Aladdin	F121152
Critical commercial assays		
Calcein-AM/PI double stain kit	Dojindo	C542
Cell Counting Kit-8 assay	Beyotime Biotechnology	C0043
Mesenchymal stem cell growth medium kit	Cyagen	HUXMF-90011
Matrix metallopeptidase 2 protein ELISA kit	Beyotime Biotechnology	PM730
Experimental models: Cell lines		
Immortalized human corneal epithelial cells	RIKEN Biosource Center	N/A
Immortalized HCEnd cells	Applied Biological Materials Inc.	T5077
Bone marrow-derived mesenchymal stem cells	Cyagen	HUXMF-01001
Software and algorithms		
Image Pro Plus	Media Cybernetic Inc.	6.0
GraphPad Prism	GraphPad Software Inc.	Prism 8
MATLAB	MathWorks	R2019a

RESOURCE AVAILABILITY

Lead contact

Further information and requests for resources should be directed to Prof. Hui Yang (hui.yang@siat.ac.cn).

Materials availability

This study did not generate new unique reagents.

Data and code availability

All data needed to evaluate the conclusions in the paper are present in the paper and the supplemental information. This paper does not report the original code. Any additional information required to reanalyse the data reported in this paper is available from the lead contact upon request.

EXPERIMENTAL MODEL AND SUBJECT DETAILS

Immortalized HCEpi cells were obtained from RIKEN Biosource Center, and then cultured in DMEM/F-12 basal medium and supplemented with fetal bovine serum (FBS), 10 ng/mL human EGF and 1% penicillin-streptomycin. Immortalized HCEnd cells were maintained in Prigrow I medium supplemented with 10% FBS, 5 mg/L human insulin, 10 μg/mL human transferrin, 3 ng/mL sodium selenite, 10 nM hydrocortisone, 10 nM β-estradiol, 10 ng/mL human VEGF 165aa, 10 ng/mL human EGF, 10 ng/mL Heparin, 1% L-glutamine, and 1% penicillin-streptomycin. BM-MSCs were grown in MSC Growth Kit Medium according to the manufacturer's protocols. The cells were grown at 37°C in a 95% humidified 5% CO_2 incubator and used at low passage numbers.

METHOD DETAILS

H&E (H&E) staining of the corneal epithelium

For histological analysis of differentiated corneal epithelium, the cells on the membrane were fixed by 4% paraformaldehyde (PFA) for 30 min and incubated in PBS (PBS) overnight at 4°C. Then the membrane was carefully removed from the PDMS device for further processing. For tissue dehydration, low-to high-concentration alcohol was used to remove water from the tissue gradually. Subsequently, the dehydrated film was incubated with xylene for 30 min to be transparent and then transferred to a mixture of molten paraffin wax for incubation at 56°C for 30 min and then in 100% molten wax for another 60 min twice. After embedding, the membrane was sectioned into slices of 4 μm in thickness.

For H&E staining, the paraffin-embedded sections were deparaffinized first in a clearing agent and rehydrated from high-to low-concentration ethanol. After rinsing in distilled water for 1 h, the sections were stained with hematoxylin for 1 min and then washed with tap water for 3 min, followed by treating with Scott's buffer for 30 sec, rinsing in tap water for 3 min, and staining with eosin for 40 sec. Finally, the slides were rinsed with 95% ethanol twice for 1 min each, 100% ethanol for 1 min, and the clearing agent for 1 min. The slides were finally mounted and sealed with a coverslip for further characterization.

Measurement of corneal permeability

The device was equilibrated with sterile Hanks balanced stock solution (HBSS) in the incubator for 20 min. Then, the solution in the upper channel was replaced with HBSS containing fluorescently labeled dextran at a concentration of 100 μg/mL. The levels of solution in both the upper and the lower compartment were equalized to avoid pressure-driven fluid flow. Sample solutions were collected from the outlet reservoir of the lower channel at 1 h post-dosing and read by a Microplate Reader. Before data analysis, a calibration curve was established by measuring nine standard concentrations of FITC-Dextran prepared in HBSS, covering a dynamic range of 0–100 μg/mL (see Figure S5). Using this calibration curve, the concentration of FITC-Dextran in the solution collected from the lower channel can be obtained. A device unseeded with cells was used as the "Control" group, whose data was subtracted from all readings before data analysis. The permeability coefficient (Papp) of epithelium or cornea-chip was calculated by

$$P_{app} = \frac{dQ}{dt} \times \frac{1}{AC_0}$$

Where, dQ/dt is the slope of the cumulative fraction absorbed versus time (in seconds), A is the area of the culture zone (cm^2), and C_0 is the initial concentration in the apical chamber (μg/mL).

Immunofluorescence staining of corneal cells

The cells on the cornea-chip were firstly washed with PBS and fixed with 4% PFA for 30 min. The membrane was then carefully removed from the device and transferred into a well plate for further processing. The membrane was permeabilized with 0.25% Triton X-100 for 10 min, blocked by 1% BSA for 1 h at room temperature, incubated with a primary antibody overnight at 4°C, and stained by a secondary antibody for 1 h. Detailed information on the antibodies used in our study is provided in Key resources table. Nucleus staining was performed using 2 μg/mL 4′,6′-diamidino-2-phenylindole hydrochloride (DAPI) for 10 min. The membrane was then placed between coverslips using a fluorescent mounting medium and photographed by a Zeiss Axio Observer seven fluorescent microscope. The mean fluorescence intensity (MFI) of protein expression was analyzed by Metlab R2019a.

EVs isolation

Differential ultracentrifugation was used for EVs isolation. Briefly, the cell culture medium was collected after centrifugation of the cell culturing medium at 500 g for 10 min. The supernatant was then centrifuged using 2,000 g for 15 min at 4°C to avoid cell debris. The supernatant was collected at 10,000 g for 30 min at 4°C. The medium was extracted and further purified at 100,000 g for 70 min at 4°C in JXN-30 Ultracentrifuge. The EVs pellet was resuspended in 100 μL PBS for further use. More details on EVs' characterization is presented in the Supporting Information (Figure S6).

Scratch wound healing assay

After the HCEpi cells were grown confluently on the membrane in the chip, a 200 μL pipette tip was used to make a scratch wound on the epithelium layer. Scraped cells were removed by rinsing with PBS, and the cells were stained using 2 μg/mL DAPI for 10 min and photographed at time 0. Cells were incubated on-chip by different media at volumetric flow rate of 100 μL/h, the serum-free culture medium and EVs isolated from BM-MSCs (MSC-EVs) were used as the control and the experimental group, respectively. After 24 h, the wounds treated with different media were again photographed, and the margins of the wound area were traced. The area was quantified using ImagePro Plus software and compared to the wound area at time 0.

ELISA

Human MMP-2 protein in the HCEpi and HCEnd cells cultured on chip was quantitated using a sandwich ELISA (ELISA). The experimental procedures followed the manufacturer's protocols. Each experimental group was tested three times for data analysis. A calibration curve was obtained by testing serial dilutions of human MMP-2 protein. Light absorption was measured at 450 nm on a Microplate Reader. The lower limit of sensitivity for this ELISA kit was 0.625 ng/mL.

QUANTIFICATION AND STATISTICAL ANALYSIS

All results were presented as mean ± SD (SD). The unpaired t-test or two-way ANOVA followed by Bonferroni's multiple comparisons test was performed using GraphPad Prism 8. All data were obtained from three individual experiments, and each experiment was tested on six devices. The p values are obtained from source data and reported in figure legends. "ns" no significant difference, "*" $p < 0.05$, "**" $p < 0.01$, "****" $p < 0.0001$.